

Two-dimensional phase cycled reconstruction for inherent correction of EPI Nyquist artifacts

N.-K. CHEN¹, A. V. AVRAM¹, AND A. W. SONG¹

¹BRAIN IMAGING AND ANALYSIS CENTER, DUKE UNIVERSITY MEDICAL CENTER, DURHAM, NC, UNITED STATES

INTRODUCTION

The inconsistency of k-space trajectories corresponding to opposite frequency-encoding gradient polarities in echo-planar imaging (EPI) results in Nyquist artifacts. Traditional techniques often only correct for phase errors along the frequency-encoding direction (i.e., 1D correction), which may still leave significant residual artifacts, particularly for oblique-plane EPI or in the presence of cross-term eddy current. As compared with 1D correction, two-dimensional (2D) phase correction methods can be much more effective in suppressing Nyquist artifacts. However, most existing 2D correction methods require extra reference scans and may not be generally applicable to different imaging protocols (e.g., cardiac MRI) [Chen: MRM 51(6), p.1247; 2004]. To address this limitation, we report an inherent 2D phase correction technique for EPI Nyquist removal. First, a series of images are generated from the same original dataset, by cycling through different possible values of phase errors using a 2D reconstruction framework. Second, an image with the lowest artifact level is identified from multiple generated images using criteria based on background energy in sorted and sigmoid-weighted signals.

THEORY AND METHODS

The N-shot EPI k-space data are first decomposed into 2N subset. For example, the two-shot EPI data can be decomposed into four subsets corresponding to 1) segment #1 / positive frequency-encoding gradient (S1+), 2) segment #2 / positive gradient (S2+), 3) segment #1 / negative gradient (S1-), and 4) segment #2 / negative gradient (S2-). If the 2D phase errors are known a priori, then the artifact-free signals can be determined from measured signals (e.g., S1+, S2+, S1- and S2- data sets in 2-shot EPI) using Equation 1, with P_n represents un-aliased complex parent image signals separated by FOV/2N along the phase-encoding direction; u_k and v_k representing aliased image signals corresponding to the positive and negative gradient polarities of the k-th segment respectively; and ϕ_n representing the 2D phase errors at location P_n .

Here we integrate the 2D EPI phase correction procedure with an iterative column-based phase cycled reconstruction without the need of *a priori* 2D phase information. In our implementation we assumed that 2D phase errors are consisted of 1) a spatially-independent phase offset, 2) nonlinear terms along the frequency-encoding direction, and 3) linear terms along the phase encoding direction. Specifically, the 2D phase errors in a chosen column (at location x_0 along the frequency-encoding direction) can be represented by $\phi(x_0, y) = C_1 + C_2 \times y$, where C_1 includes the contribution from both 1) a phase offset that is uniform for the whole 2D image, and 2) nonlinear phase terms along the frequency-encoding direction; C_2 represents the linear phase gradient along the phase encoding direction.

We then generated multiple sets of 1D profiles with Equation 1, based on different possible values of C_1 (cycled between $-\pi$ and $+\pi$ in 50 steps) and C_2 (between $-\pi$ per pixel and $+\pi$ per pixel in 50 steps). In other words, 2500 sets of 1D signals were generated from this chosen column. The 1D profile (from 2500 profiles) that is among the lowest artifact level is identified in four steps: 1) The 1D signals generated from one of the phase patterns are sorted in an ascending order; 2) The sorted 1D profiles are multiplied by a sigmoid function, suppressing signals in ~80% of FOV; 3) The sorted and sigmoid-weighted signals are summed; and 4) The 1D profile with the lowest summed signal is identified from profiles corresponding to different combinations of coefficients C_1 and C_2 . For example, the left and right panels of Figures 1a show the 1D magnitude profiles of phantom EPI data generated from two different sets of C_1 and C_2 values. The sorted signals are presented by solid curves in Figure 1b, showing that more energy exists under the unsuppressed region of a sigmoid window (red dashed curve) in the left panel as compared with the right panel. The sigmoid-weighted signals are shown in Figure 1c, indicating a higher artifact level in the left panel than in the right panel. Based on the criteria, 2D images with lower artifact level can be automatically generated (Figure 1d: right panel).

IN VIVO EXPERIMENTS AND RESULTS

The human brain EPI data (3 Tesla) in double oblique plane, acquired with 1, 2, 4, and 8 segments are shown in Figures 2a to 2d, respectively. The images in the left column of Figure 2 were reconstructed directly from the k-space data with Fourier transform without any phase correction, and show strong Nyquist artifacts in all four data sets. The images in the middle column of Figure 2 were reconstructed with 1D phase correction and exhibit significantly reduced artifacts as compared with uncorrected images. However, residual artifacts remain visible and may interfere with the parent image signals, as indicated by arrows. The images in the right column of Figure 2 were reconstructed with the new 2D phase correction technique without the need of any reference scan. It can be seen that Nyquist artifacts are much better suppressed with 2D correction in comparison to those with the conventional 1D correction method. The ghost-to-noise ratios measured from the manually chosen ROIs were 4.6 in 1D phase-corrected images, and 2.3 for 2D phase-corrected images.

In conclusion, in this report we present an inherent 2D phase correction technique, for effectively reducing Nyquist artifacts in single-shot and multi-shot EPI, without needing any reference scan. The developed method is generally applicable to full-Fourier, partial-Fourier, and parallel EPI.

$$\begin{bmatrix} u_1 \\ u_2 \\ \vdots \\ u_N \\ v_1 \\ v_2 \\ \vdots \\ v_N \end{bmatrix} = \frac{1}{2N} \begin{bmatrix} e^{i\frac{\pi}{N}0\cdot0} & e^{i\frac{\pi}{N}0\cdot1} & \cdots & e^{i\frac{\pi}{N}0\cdot(2N-1)} \\ e^{i\frac{\pi}{N}1\cdot0} & e^{i\frac{\pi}{N}1\cdot1} & \cdots & e^{i\frac{\pi}{N}1\cdot(2N-1)} \\ \vdots & \vdots & \ddots & \vdots \\ e^{i\frac{\pi}{N}(N-1)\cdot0} & e^{i\frac{\pi}{N}(N-1)\cdot1} & \cdots & e^{i\frac{\pi}{N}(N-1)\cdot(2N-1)} \\ e^{i\frac{\pi}{N}N\cdot0} e^{i\phi_1} & e^{i\frac{\pi}{N}N\cdot1} e^{i\phi_2} & \cdots & e^{i\frac{\pi}{N}N\cdot(2N-1)} e^{i\phi_{2N}} \\ e^{i\frac{\pi}{N}(N+1)\cdot0} e^{i\phi_1} & e^{i\frac{\pi}{N}(N+1)\cdot1} e^{i\phi_2} & \cdots & e^{i\frac{\pi}{N}(N+1)\cdot(2N-1)} e^{i\phi_{2N}} \\ \vdots & \vdots & \ddots & \vdots \\ e^{i\frac{\pi}{N}(2N-1)\cdot0} e^{i\phi_1} & e^{i\frac{\pi}{N}(2N-1)\cdot1} e^{i\phi_2} & \cdots & e^{i\frac{\pi}{N}(2N-1)\cdot(2N-1)} e^{i\phi_{2N}} \end{bmatrix} \begin{bmatrix} P_1 \\ P_2 \\ \vdots \\ P_{N-1} \\ P_N \\ P_{N+1} \\ \vdots \\ P_{2N} \end{bmatrix} \quad \text{Eq 1}$$

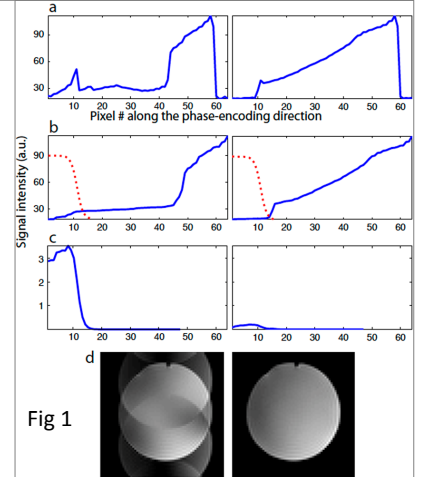


Fig 1

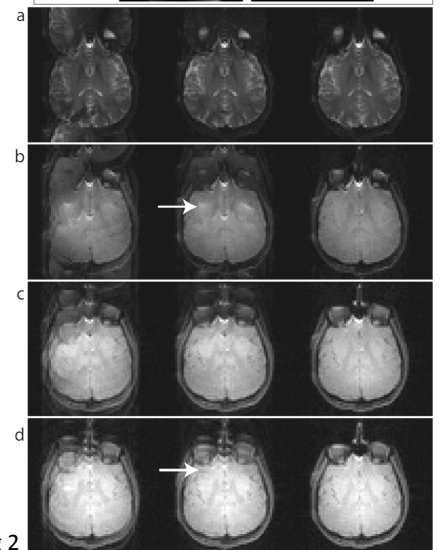


Fig 2